Improving the stability, selectivity, and cell voltage of a bipolar membrane zero-gap electrolyzer for low-loss CO_2 reduction

Bhavin Siritanaratkul[a], Preetam K. Sharma[b], Eileen H. Yu[b], and Alexander J. Cowan[a]*

[a] Dr. B. Siritanaratkul, Prof. A. J. Cowan
Stephenson Institute for Renewable Energy and the Department of Chemistry
University of Liverpool
Liverpool, L69 7ZF, UK
E-mail: acowan@liverpool.ac.uk
[b] Dr. P. K. Sharma, Prof. E. H. Yu
Department of Chemical Engineering
Loughborough University
Loughborough, LE11 3TU, UK

Supporting information for this article is given via a link at the end of the document.

Abstract: Electrolyzers for CO_2 reduction containing bipolar membranes (BPM) are promising due to low loss of CO_2 as carbonates and low product crossover, but improvements in product selectivity, stability, and cell voltage are required. In particular, direct contact with the acidic cation exchange layer leads to high levels of H_2 evolution with many common cathode catalysts. Here we report Co phthalocyanine (CoPc) as a suitable catalyst for a zero-gap BPM device, reaching 53 % Faradaic efficiency to CO at 100 mA cm^{-2} using only pure water and CO_2 as the input feeds. We also showed that the cell voltage can be lowered by constructing a customized BPM using TiO_2 water dissociation catalyst, however this was at the cost of decreased selectivity. Switching the pure-water anolyte to KOH improved both the cell voltage and CO selectivity (62% at 200 mA cm^{-2}), but cation crossover could cause complications. Our results demonstrate viable strategies for improving a BPM CO_2 electrolyzer towards practical-scale CO_2-to-chemicals conversion.

Introduction

Electrochemical CO_2 reduction, combined with electricity from renewable sources, is a key technology to achieve Net Zero by converting waste CO_2 into valuable chemicals, thus enabling a closed-loop carbon cycle.[1] To achieve practical-scale CO_2 reduction, we need to consider not only metrics of the electrolyzer itself (current density, Faradaic efficiency), but also other components in the process such as product separation. In a well-studied configuration, flow cells with gas diffusion electrodes (GDE) using an alkaline catholyte and an anion-exchange membrane (AEM) can reach very high current densities and Faradaic efficiency for carbon products,[2] but this cell configuration has an inherent problem in the parasitic reaction of feed CO_2 with hydroxides, forming carbonates.[3] The problem is threefold: a) carbonates formed in the catholyte needs to be regenerated to CO_2, at an energetic penalty, for recycling of the CO_2 feed, b) the generated carbonates act as the charge carrier through the AEM, resulting in CO_2 crossover to the anode stream and increasing separation costs,[3] and c) carbonates can precipitate out and cause blockages in the GDE.[4]

Various cell configurations have been proposed to circumvent the carbonate formation problem.[5] One of the most promising configurations is an electrolyzer with a bipolar membrane (BPM), which is composed of a cation-exchange layer (CEL) and an anion-exchange layer (AEL). BPMs can mitigate carbonate formation, as well as CO_2 and product crossover,[6] and in addition it allows steady-state operation at different pHs at the cathode and anode.[7] In the forward-bias BPM configuration, the AEL is towards the cathode, and carbonate and hydroxide ions are transported through the AEL.[8] While having the AEL towards the cathode can provide a local alkaline environment (thus enabling high Faradaic efficiency for carbon products), the generation of water and/or CO_2 at the CEL/AEL interface can potentially lead to blistering and delamination of the BPM.[9]

In contrast, in the reverse-bias BPM configuration, the CEL is towards the cathode, and water dissociation occurs at the CEL/AEL interface. Typical metal catalysts (e.g. Ag, Cu) in direct contact with an acidic CEL leads to significant H_2 evolution and low selectivity towards carbonaceous products.[10] Various methods to improve the selectivity have been demonstrated in the literature, for example by adjusting the acidity of the CEL,[11] inserting a solid-supported bicarbonate buffer layer,[12] or a non-buffering electrolyte layer.[13]

We recently reported a zero-gap CO_2 electrolyzer with a reverse-bias bipolar membrane.[14] By using molecular catalysts (Ni(cyclam), cyclam = 1,4,8,11-tetraazacyclotetradecane, or its carboxylic acid derivative) known for selective CO_2 reduction to CO in low pH conditions, we achieved relatively high CO faradaic efficiency (63 % at 25 mA cm^{-2}) compared to metallic Ag catalysts, and the device operated with only CO_2 and pure water as feeds. The intrinsic catalyst selectivity avoids the use of a pH buffering layer and high alkali salt concentrations which is potentially beneficial as salt precipitation is completely avoided. However, the full cell voltages were relatively high, and Ni cyclam was affected by product inhibition and eventual degradation which led to low stability (on a scale of <1 h).

In this work, we report strategies to improve both the stability and cell voltages of this electrolyzer configuration. Co-based molecular catalysts for CO_2 reduction have been reported, mainly comprising a phthalocyanine or porphyrin ligand or their derivatives.[15] While the majority of studies were conducted in alkaline conditions (either alkaline electrolyte or an AEM zero-gap cell), some studies have reported these catalysts operating in acidic conditions, albeit at lower current densities and only in an H-cell configuration.[16] Here we chose Co phthalocyanine (CoPc), supported on carbon, as the cathode catalyst and demonstrated that it can be used at high current densities (up to 200 mA cm^{-2}) with good selectivity's in an acidic environment. The introduction of water dissociation (WD) catalysts into the CEL/AEL junction

can enhance WD and thus lower the cell voltage, and here we report the effects of using a customized BPM, as well as the analysis of various voltage loss pathways by electrochemical impedance spectroscopy. Figure 1 shows a diagram of the cathode and BPM, and the structure of CoPc.

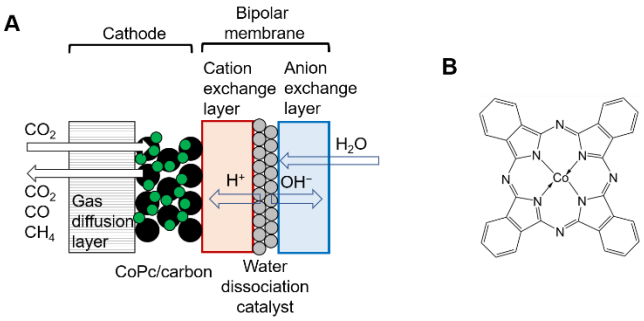

Figure 1. A) Diagram of the cathode with a bipolar membrane in a reverse-bias configuration. B) chemical structure of Co phthalocyanine (CoPc).

Results and Discussion

First, we show the overall performance of the zero-gap BPM cell (commercial Fumasep FBM membrane) with CoPc as the cathode catalyst. The cathode was constructed by spraying CoPc supported by carbon powder (17 wt% CoPc, total loading 1.2 mg/cm^2, for full experimental details see methods) onto carbon paper (5 cm^2). The CoPc/carbon cathode was cold-pressed in the electrolyzer cell, together with the BPM and a RuO_2 anode, with the CEL of the BPM towards the cathode (reverse-bias configuration). We used a pure H_2O feed at the anode, to avoid possible co-ion transport and crossover of ions which could convolute the performance at the cathode.[17] In reverse biased BPM studies an alkaline electrolyte (e.g. 1 M KOH) is sometimes used at the anode and this should lower the overall cell voltage further, but crossover of K^+ can influence the cathode behaviour (see below).

Figure 2A shows the initial faradaic efficiencies to H_2 and CO, obtained during 2-electrode chronopotentiometric measurements. The FE for CO reached 69±4 % at a total current density of 25 mA cm^{-2}, decreasing to 50±2 % at 100 mA cm^{-2} and 34±2 % at 200 mA cm^{-2}. The selectivity reached here is a large improvement over our previous report with Ni cyclam and its derivative in the same cell configuration (~20-30 % at 100 mA cm^{-2}),[14] mainly because CoPc does not show noticeable product inhibition by CO and subsequent reductive deactivation. The CoPc also significantly outperforms the previously reported Ag nanoparticle benchmark catalyst in this cell configuration (20±2 % at 100 mA cm^{-2}).[14] Figure 2B shows the full cell voltages and the CO partial current densities. A breakdown of the cell voltage and its improvement is discussed further below. Linear sweep voltammograms of the cell, comparing CoPc/carbon and blank carbon cathodes, are shown in Figure S1. Under Ar, the blank carbon cathode showed activity towards hydrogen evolution reaction (HER), which is suppressed under CO_2, as also observed by Burdyny and coworkers.[18] Interestingly, in contrast to Ag in their study, which showed increased HER throughout the potential range, CoPc under Ar showed suppressed HER at lower currents compared to the blank, indicating that CoPc has intrinsic higher overpotential for HER under our zero-gap acidic cathode environment.

The CO partial current density increased towards a plateau with total current density, reached 68±3 mA cm^{-2} at 200 mA cm^{-2} total current density. The plateau in CO partial current density is presumably due to the intrinsic turnover frequency of CoPc and total electroactive content (also observed in previous work using Ni-based molecular catalysts[14]), and not due to mass transport limitations (see below for CO_2 flow rate dependence). We measured the electroactive coverage by cyclic voltammograms of a fresh CoPc/carbon on carbon paper electrode (see SI Figure S2), we observed clear peaks at ~-0.25 V vs SHE in 0.1 M $KHCO_3$,[19] and obtained a coverage of approximately 3.8 × 10^{-8} mol cm^{-2} for a fresh cathode. Using this electroactive coverage, we calculate the maximum turnover frequency (TOF) achieved (from the maximum CO partial current density) to be 12 s^{-1}, which is comparable to literature.[15b] (We note that there is a large spread in the reported coverage and TOF values, as this is heavily influenced by preparation methods and cell configurations). As a minor product, CH_4 was also observed, but at the levels of <0.1 % Faradaic efficiency. A small amount of CH_4 was previously reported on a Co-protoporphyrin complex[20] in acidic electrolyte (~0.1 % FE at ambient conditions, rising to 2% with 10 atm CO_2). The CH_4 is generated from further protonation and reduction of the adsorbed CO, and while this is promoted under acidic conditions, the contribution of this pathway is still small relative to CO generation and desorption.

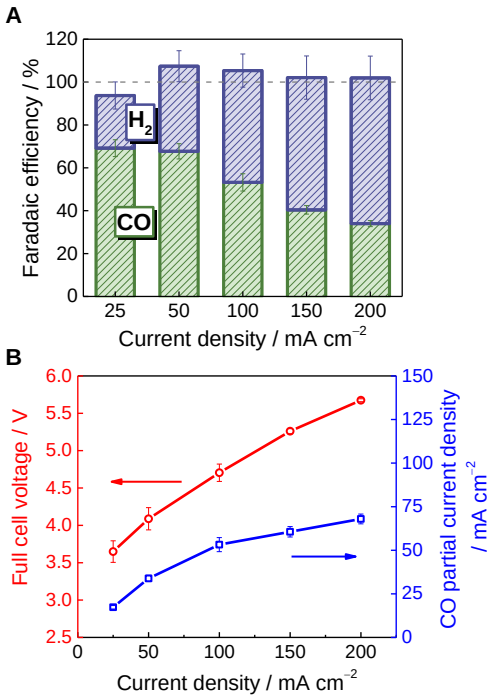

Figure 2 Performance of CoPc/carbon in a reverse-bias zero-gap BPM electrolyzer. A) Initial Faradaic efficiency towards CO and H_2, and B) Full cell voltage (red, left axis) and CO partial current density (blue, right axis) as a function of total current density. Conditions: Cathode area 5 cm^2, cathode feed: CO_2 saturated by a water bubbler, 20 sccm, anode RuO_2 9 cm^2, anolyte pure water, recirculated at 15 mL min^{-1}, Membrane Fumasep FBM, room temperature, Error bars correspond to 1 standard deviation, from 3 independent samples.

We conducted longer measurements at 25 and 100 mA cm^{-2} (Figure 3). At 25 mA cm^{-2}, there was an initial decline in CO FE but it stabilised at ~40 % which was sustained for the duration of

the experiment with no further decreases (up to 4 h tested). For the run at 100 mA cm^{-2}, the selectivity reached ~30% after 3 h. As for cell voltage, we note that this commercial BPM (Fumasep) is not designed for operation at high current density at reverse bias (> 100 mA cm^{-2}) for long periods, and the voltage increase with time at 100 mA cm^{-2} is partly attributable to membrane degradation. The decrease in cell voltage at 25 mA cm^{-2} is not due to the shift towards H_2 production, since the selectivity was stable after the initial drop, but rather due to change in hydration of the membrane or the electrodes after commencing operation. (See below for impedance analysis of cell voltage). Pausing the applied current (while keeping the CO_2 and H_2O feed on) had no effect in restoring the selectivity, indicating that the partial loss in selectivity is not due to product inhibition or catalyst desorption, since in both cases we would expect some recovery in CO selectivity, either due to CO being flushed out, or catalyst re-adsorption, during the pause period. Overall the stability of the CoPc cathode is a large improvement on the past Ni cyclam catalyst where activity at both 25 and 100 mA cm^{-2} was limited to < 1 hour.

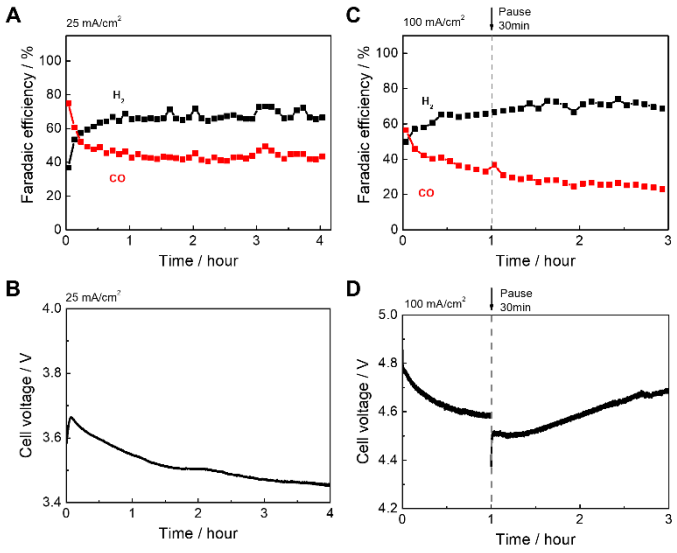

Figure 3 Stability of the product selectivity and cell voltage of CoPc/carbon in a reverse-bias zero-gap BPM electrolyzer at A,B) 25 mA cm^{-2} and C,D) 100 mA cm^{-2}.Conditions: Cathode area 5 cm^2, cathode feed: CO_2 saturated by a water bubbler, 20 sccm at inlet, anode RuO_2 9 cm^2, anolyte pure water, recirculated at 15 mL min^{-1}, Membrane Fumasep FBM

One possible cause of selectivity decrease is the partial flooding of the gas diffusion layer (GDL) of the cathode, which could result in lower CO_2 supply to the catalyst. Flooding can occur irrespective of carbonate formation, due to water transport through the BPM as well as water formation as part of the reaction of CO2 conversion to CO. Periodic drying has been shown to help sustain the activity of CoPc on GDEs at higher pH's.[21] In a separate experiment, we measured the double layer capacitance of the cathode (as a quantification of water penetration into the GDE)[22] by cyclic voltammetry. Initially, after preconditioning, the cathode capacitance was 51 µF cm^{-2}, which increased to 514 µF cm^{-2} after chronopotentiometry at 100 mA cm^{-2} for 2 h. During this period, the CO Faradaic efficiency decreased from 42 % to 18 %. The cell was then disassembled and the cathode taken out to dry in ambient air overnight, and after reassembly the capacitance decreased to 306 µF cm^{-2}. When the chronopotentiometry was restarted at 100 mA cm^{-2}, there was a concomitant recovery of CO FE to 41%, which then declined again during operation, thus confirming that at least part of the selectivity decline is due to flooding.

Another possible cause of selectivity decrease is the demetallation of Co from CoPc.[23] To observe the chemical nature of the CoPc catalyst, we conducted X-ray photoelectron spectroscopy (XPS) measurements of the fresh and used (at 100 mA cm^{-2}, 'short' = 0.5 h, 'long' = 4 h) cathodes, and for reference, XPS of CoPc powder was also measured using the same parameters (Figure 4). Signals assigned to Co^{2+} in CoPc were clearly observed in both fresh and used samples. The peaks at 781.1 eV and 796.6 eV correspond to Co $2p_{3/2}$ and Co $2p_{1/2}$, respectively. The positions of the peaks and spin-orbit separation of 15.5 eV between them matches well with the literature.[24] The peak at 783.0 eV is assigned to multiplet splitting of Co which occur due to the unpaired electrons in the valence level. The peak could not be the satellite contribution because for it to be satellite, there should have been a satellite contribution from Co $2p_{1/2}$ also, which is absent.[25] The accompanying C 1s and N 1s spectra are shown in the SI (Figure S3), and these are consistent with CoPc on a carbon paper substrate, with contributions of C-F signals due to the added Nafion in the cathode ink.

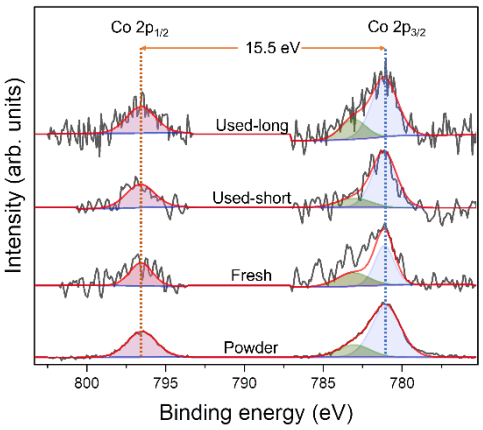

Figure 4. Co 2p XPS spectra of CoPc cathode at various stages of the analysis. Spectrum of the CoPc powder is shown for reference.

We also conducted ex-situ scanning electron microscopy and energy dispersive X-ray (SEM/EDX) of the fresh and used (100 mA cm^{-2}, 4 h) cathode (Figure S4, Table S2). The Co signals were clearly observed and relatively well-distributed on the µm scale, for both fresh and used samples. As a semiquantitative measure, we used the signal of Co normalized by that of F, which is assumed to be similar across the samples (due to the background Nafion and PTFE present in the carbon paper), and found that the Co:F atomic ratio was slightly decreased from 0.090 (fresh) to 0.072 (used 30 min and 4 h), indicating that a small amount of Co was lost during operation. This is also observed in the decreased electroactive coverage of CoPc in the used sample (Figure S2). Taken together with the sustained CO selectivity (Figure 3), the characterization (XPS and EDX) indicates that although some loss of Co did occur, a substantial portion of CoPc still remained active on the cathode after operation at 100 mA cm^{-2} for 4 h. From the capacitance measurements and post-run characterization, we

conclude that the decline in selectivity is due to both GDL flooding (leading to decreased CO_2 supply to CoPc), and CoPc demetallation. Water management and GDL flooding are critical issues in zero-gap electrolyzers,[4a, 26] and future work on membrane water transport and cathode hydrophobicity is needed.

A key performance metric is the CO_2 utilization efficiency, or single-pass yield of carbon products (defined as the proportion of inlet CO_2 that was converted into the desired carbon products, CO in this case). (Note that this has also been referred to as single-pass conversion in the literature, although this is a potentially confusing usage if CO_2 can also be converted into undesired products, i.e. carbonates). At constant current (100 mA cm^{-2}), we varied the inlet CO_2 flow rate and measured the CO Faradaic efficiency and the CO single pass yield (Figure 5A). This was conducted on the same sample, measured after the initial drop in selectivity (after ~1 h) such that the performance is relatively stable. The CO Faradaic efficiency only decreased slightly with lower inlet flow rates, resulting in a maximum of 51 % CO yield at 3 sccm inlet flow. This is comparable to the carbon product yield of a recently reported BPM system with a Cu cathode (~20 – 60 % at similar inlet flow rates).[13] There is a trade-off between CO productivity (measured in amount of CO produced per unit time) and the CO yield, which was analysed by Hawks and coworkers.[27] Higher inlet flow results in higher productivity (defined as moles or mass of CO produced per unit time), because higher CO_2 flow lessens the effect of CO_2 depletion but this comes at a cost of lower percentage yield due to dilution of the product stream. We illustrate this trade-off in Figure 5B, for 25 and 100 mA cm^{-2}, together with trendlines obtained from least-squares fitting to the relationship reported in Hawks et al.. The more scattered fit at the higher current is due to degradation during the measurement (conducted in the order 10, 3, 40, 5, 20 sccm).

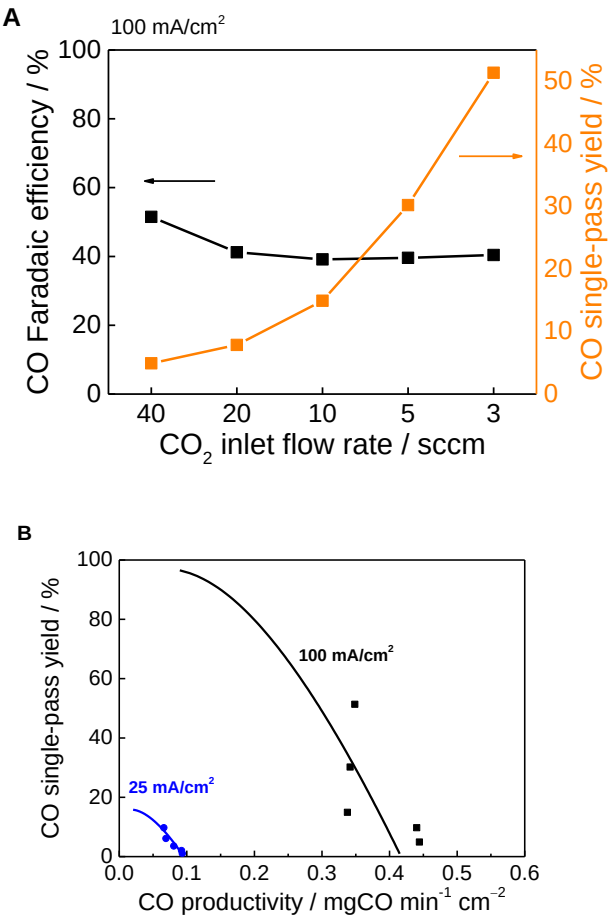

Figure 5 A) Dependence of CO Faradaic efficiency (black, left axis) and CO single-pass yield (orange, right axis) on the CO_2 inlet flow rate. B) Trade-off between CO single-pass yield and CO productivity, at 25 mA cm^{-2} (blue) and 100 mA cm^{-2} (black). Conditions: Cathode CoPc/carbon area 5 cm^2, cathode feed: CO_2 saturated by a water bubbler, anode RuO_2 9 cm^2, anolyte pure water, recirculated at 15 mL min^{-1}, Membrane Fumasep FBM

Up to this point, we have been using a commercially-available BPM (Fumasep FBM). However, the full cell voltages remain high (~4.7 V at 100 mA cm^{-2}). In addition, this commercial Fumasep BPM is not suited for long-term operation at >100 mA cm^{-2}, according to the supplier. This has resulted in variation in cell voltage after long operation, as well as batch-to-batch differences. The voltage requirement of a BPM electrolyzer depends on the ion transport characteristics of the CEL and AEL, and the rate of water dissociation (WD) at the CEL/AEL junction. The addition of catalysts (e.g. metal oxides, graphene oxide) has been shown to increase the WD rate at the junction, leading to higher currents during reverse-bias operation.[28]

Here, we constructed a custom BPM composed of a Nafion 117 membrane as the CEL, a Sustainion X37-50 membrane as the AEL, and TiO_2 (anatase) particles as WD catalysts at the CEL/AEL junction (at a loading of 30 µg cm^{-2} by airbrushing). Figure 6A compares the CO FE obtained from this custom BPM to the commercial Fumasep BPM (from Figure 2A). The cathode and anode remained the same CoPc/carbon and RuO_2, respectively. The CO selectivity using the custom BPM was significantly lower than the Fumasep BPM throughout the current density range measured here, we believe this is because it

generated a more acidic local environment at the cathode compared to the Fumasep BPM. Whilst we can reasonably conclude that the increased hydrogen evolution is due to a change in pH, as noted alongside Figure S5, the local proton concentration is due to a number of factors meaning the cause of can't be readily ascertained.

Future improvements to the selectivity can be expected, for example by modifying the acidity of the CEL, or by inserting a thin intervening layer between the CEL and the cathode. The comparison of cell voltages is shown in Figure 6B. A custom BPM with no WD catalyst showed very high cell voltages (>7 V at 30 mA cm^{-2}), demonstrating that TiO_2 was effective in promoting water dissociation. Overall, the cell voltage from the custom BPM with a TiO2 WD catalyst was ~0.5 – 0.8 V lower than that of the commercial Fumasep membrane.

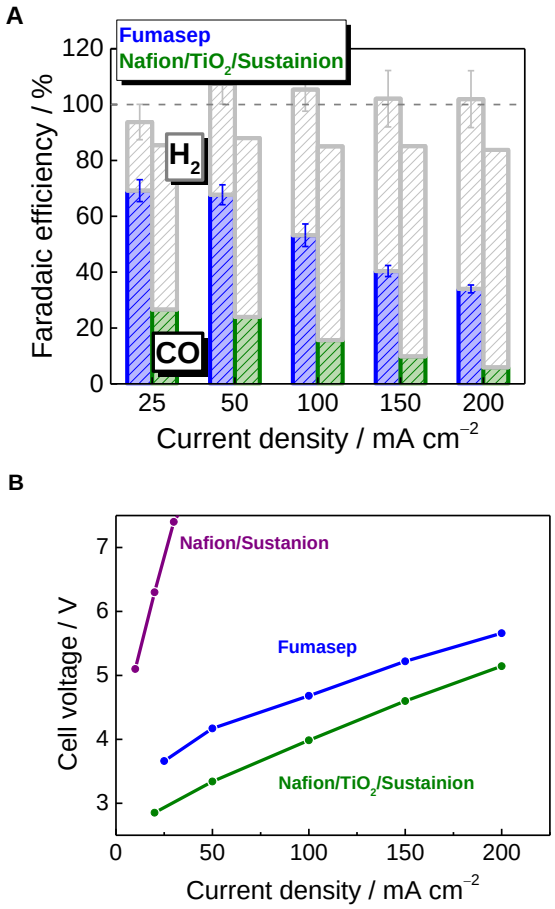

Figure 6 A) CO Faradaic efficiency of a custom BPM (Nafion/TiO_2/Sustainion) (green) and a commercial Fumasep FBM (blue, from Figure 2). Conditions: Cathode CoPc/carbon area 5 cm^2, cathode feed: CO_2 saturated by a water bubbler, 20 sccm, anode RuO_2 9 cm^2, anolyte pure water, recirculated at 15 mL min^{-1}

To identify the contributions of various processes, we conducted electrochemical impedance spectroscopy (EIS) measurements at various operating current densities. Previous work by Chen et al.[28a] deconvoluted 2 processes, and attributed the higher-frequency and lower-frequency semicircles to the water dissociation at the BPM (R_{WD}), and charge-transfer at the electrodes (R_{CT}), respectively. Here we also observe 2 semicircles, and fitted each of the process to a constant-phase element (CPE), for a non-ideal capacitive element, in parallel to a resistance element (Figure 7A). We term the high-frequency intercept the cell resistance (R_{cell}), and this comprises the cell plates and contacts, the ionic transport through the membranes, and the resistance of the WD catalyst layer itself. Figure 7A shows the Nyquist plot of the resistance-area product (the real and imaginary parts of the impedance normalized by multiplying the cathode area) of the cell with either the commercial Fumasep or the custom BPM (Nafion/TiO_2/Sustainion) under operation at 25 mA cm^{-2}, which gives a reasonable fitting with the circuit in Figure 7A. The EIS measurement was conducted at operating current density 25 – 200 mA cm^{-2} and Figure 7B,C shows these resistances (R_{cell}, R_{WD}, R_{CT}) for the Fumasep and the custom BPM. The deconvolution of these 3 resistances allowed a breakdown of the overall cell voltage (Figure 7D,E).

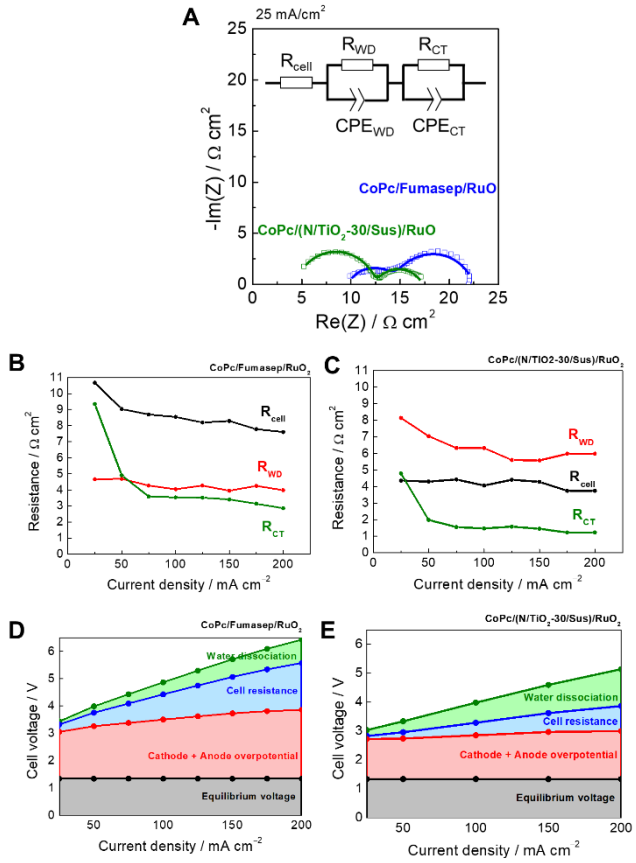

Figure 7 Electrochemical impedance spectroscopy (EIS) and cell voltage breakdown of the commercial Fumasep BPM and the custom Nafion/TiO2/Sustainion BPM. A) Equivalent circuit diagram and measured (points) and fitted (line) Nyquist plot comparing the Fumasep BPM (blue) and the custom Nafion/TiO_2/Sustainion BPM (green) at 25 mA cm^{-2}. B,C) Dependence of each resistance component: cell resistance (R_{cell}, black), water dissociation (R_{WD}, red), charge transfer (R_{CT}, green), on the operating current density. D,E) Cell voltage breakdown, the voltages are summed so the green line provides the total cell voltage. Conditions: Cathode CoPc/carbon area 5 cm^2, cathode feed: CO_2 saturated by a water bubbler, anode RuO_2 9 cm^2, anolyte pure water, recirculated at 15 mL min^{-1}.

Since the cell materials, cathode, and anode are the same for all measurements, the change in R_{cell} is attributable mainly to the ionic transport properties of the membrane. For the Fumasep BPM, overall the R_{cell} was higher than that of the custom BPM, indicating that the Nafion and Sustainion membranes, taken together, showed better ionic transport properties than the Fumasep FBM. The R_{cell} of Fumasep FBM showed a slight

decrease with increasing current, unlike the custom BPM which was relatively unchanged, and we attribute this to a change in hydration with more H_2O pulled through at higher currents. We also note that our results were obtained at room temperature (20 – 22 °C), and the Fumasep FBM's stated upper limit is 40 °C, but industrial electrolyzers are operated at elevated temperatures (> 60 °C) which would be beneficial for improving the membrane ionic transport. The R_{CT} (which contains contributions from both the cathode and the anode) was lower in the custom BPM, in-line with a lower local pH at the cathode. The R_{WD} was overall slightly higher in the custom BPM, indicating that future optimization of the WD catalyst (material, loading amount, loading methods) should be able to reduce the cell voltage down even further. Both membranes were operated at room temperature for comparison, but in practice electrolyzers are typically operated at >60 °C, which should further lower both the cell and water dissociation resistances.

We measured the changes in each of these resistances, as well as the cathode capacitance, at hourly intervals during operation for 3 h at 100 mA cm^{-2} using the Fumasep membrane (Figure S6). The cell resistance remained relatively constant, and the water dissociation resistance increased slightly, while the charge transfer resistance increased noticeably, indicating possible instability at the cathode or anode. The capacitance also increased significantly, which is associated with flooding as noted above.

Finally, we investigate the effect of changing the anolyte from pure H_2O to a highly alkaline (1 M KOH) electrolyte, and the results are shown in Figure 8, using the Fumasep BPM for comparison with pure H_2O anolyte results (from Figure 2A). As expected, the cell voltage decreased by ~0.7 – 1.0 V, due to the improved anode kinetics as well as lower solution resistance. Although the cathode is separated from the anolyte, we found that CO selectivity was increased at high current density compared to using pure water anolyte (62 % vs 34 % at 200 mA cm^{-2}). A selectivity enhancement effect has been previously observed in a zero-gap BPM system with a Ag cathode when a K^+ based anolyte was used,[17] and the improvement was attributed to the crossover of cations (K^+) from the anolyte to the cathode through the BPM. The beneficial effect of cations was confirmed in a separate experiment, adding KCl directly to the CoPc/carbon cathode, while retaining pure H_2O as the anolyte (Figure S7). The extent of CO selectivity enhancement was almost identical to Figure 8A with KOH anolyte.

The effect of cations in enhancing the selectivity in CO_2 reduction is well-studied on metal cathodes, though there is still no consensus on the main cause (modification of interfacial electric field, buffering the local pH, or stabilization of an intermediate[29]). Here we also find evidence for K^+ crossover to the cathode from the anolyte (Figure S8). The cation effect is less studied on molecular catalysts, but there are reports on selectivity enhancement over CoPc[30] and Fe porphyrins[31], mainly attributed to stabilization of the M-CO_2 adduct (M is the transition metal center). Whilst this paper was in preparation a preliminary report of K^+ stabilisation of CO_2 binding at a similar Co catalyst has also been reported supporting that a cation effect may also be occurring here.[32] Future work will explore the beneficial effect of direct cation addition to the cathode, which we caution may become convoluted with potential detrimental changes associated with increased flooding and salt precipitation as a result of the K^+ crossover, Figure S9 (extended 44 hr experiment).

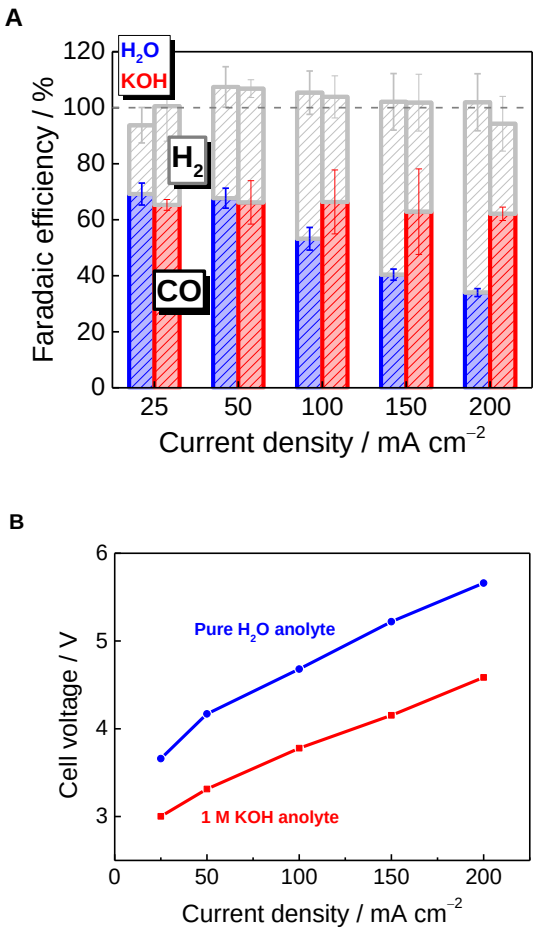

Figure 8. Effect of alkaline anolyte on cell performance with a Fumasep FBM membrane. A) Faradaic efficiency B) Cell voltage, with pure H_2O anolyte (blue) and 1 H KOH anolyte (red). Conditions: Cathode CoPc/carbon area 5 cm^2, cathode feed: CO_2 saturated by a water bubbler, anode RuO_2 9 cm^2, recirculated at 15 mL min^{-1}. Error bars correspond to 1 standard deviation, from 2 independent samples for KOH run.

Here we have shown that high Faradic efficiencies for CO production can be achieved in a reverse biased BPM electrolyzer operating at up to 200 mA cm^{-2}, despite the acidic environment, by using a CoPc molecular electrocatalyst. We have also demonstrated that a reduction in cell voltage of a BPM electrolyzer is achievable via BPM design and optimizing reaction conditions. Although the overall voltages are still higher than typical monopolar membrane (AEM) devices the costs associated with carbonate regeneration and CO_2 separation from crossover into the anode stream need to be included. CO_2 crossover losses are minimised by the use of the BPM structure and here we achieve a single-pass CO yield of 51 %. Various approaches for evaluating electrolyzers have been proposed, from simpler models considering only the energetic costs[5, 33] to more complex models involving other economic parameters such as separator cost, electrolyzer cost, plant lifetime etc.[34] Although these economic models vary with different assumptions and parameters, some of which still have large uncertainties involved due to the technology being in an early stage, systems-level analysis that take downstream processes into account suggest that BPM electrolyzers are competitive due to high CO_2 utilization

efficiencies, even when considering potentially higher cell voltages.

Conclusion

Bipolar membrane zero-gap electrolyzers are promising CO_2 reduction devices, due to low carbonate formation and crossover, which translates to high CO_2 utilization and product yield. However, challenges remain in the low selectivity, due to the acidic CEL being in direct contact with the cathode, and the additional voltage requirements for water dissociation within the BPM. Here, using only CO_2 and pure water feeds, we demonstrate that selection of CoPc as the cathode catalyst afforded a higher CO selectivity compared to previously reported benchmark Ni cyclam-based molecular catalysts and Ag metal catalysts. CoPc cathodes show stable selectivity's for CO over 4 h experiments at 25 mA cm-2. At higher current densities (100 mA cm^{-2}) there is some loss of selectivity which we propose is primarily due to partial flooding of the gas-diffusion layer. Electrochemical impedance spectroscopy led to a detailed analysis of voltage losses, which is crucial in future development of such BPMs and BPM-containing devices. Switching the anolyte from pure water to 1 M KOH improved both CO selectivity and cell voltage, proposed to be due to cation crossover however further studies are required to assess the mechanism of how KOH enhances the selectivity of this molecular catalyst cathode. Overall, this study has demonstrated strategies to improve key components of a BPM electrolyzer towards practical-scale electrochemical CO_2 conversion.

Experimental Section

Materials

Co(II) phthalocyanine (Sigma Aldrich, 97%), Ensaco 350G carbon powder (Imerys), TiO_2 (anatase, <25 nm, Sigma Aldrich, 99.7%), isopropanol (Sigma Aldrich, 99.5%), carbon paper (Sigracet 39BB), RuO_2 (FuelCellStore, nanoparticles ~5-10 nm), Fumasep FBM bipolar membrane (stored in 1 M NaCl). Nafion solution (Sigma Aldrich, 5% in a mixture of a lower aliphatic alcohols and water), CO_2 (BOC, CP grade), Nafion 117 membrane (FuelCellStore), Sustainion membrane (X37-50, Grade RT). The Fumasep FBM membrane was soaked in H_2O for 1 h prior to use. The Nafion 117 membrane was pretreated by heating in H_2O at 80°C for 2 h, then stored in H_2O. The Sustainion membrane was pretreated in 1 M KOH for 48 h at room temperature, and soaked in H_2O for 1 h prior to use. Pure water was Milli-Q grade (18.2 MΩ).

Electrode and membrane fabrication

For the cathode, first the Ensaco carbon powder was dispersed in isopropanol by sonication for 1 h, then CoPc was added then sonicated for a further 30 min. The Co/carbon suspension was left to stir overnight (~16 h), Nafion solution was added then stirred for 3 h, then sprayed (Harder & Steenbeck Evolution with a N_2 stream) onto carbon paper over a hot plate set to 40 °C. For the anode, the RuO_2 powder was dispersed in isopropanol by sonication for 1 h, then sprayed onto carbon paper over a hot plate set to 80 °C. The electrodes were left to dry in ambient air.

For the custom BPM, we adapted a procedure from the literature.[28a] TiO_2 (anatase) was suspended in a mixture of isopropanol and water then sonicated for 1 h. This suspension was sprayed onto a sheet of Nafion 117 (at a loading of 30 μg cm^{-2}), held on a glass holder on a hot plate set at 90 °C. After spraying, the TiO_2-loaded Nafion was returned to and stored in H_2O, then it was interfaced with Sustainion (with the TiO_2-loaded side in the middle) directly before assembly of the electrochemical cell.

Electrochemical measurement

Electrochemical measurements were carried out using an Ivium Vertex potentiostat. The membrane electrode assembly was assembled in the electrolyzer cell (Dioxide Materials, cathode area 5 cm^2) at ambient conditions ('cold pressing'). The Fumasep membrane was soaked in H_2O for 1 h before use. The cation exchange layer of the BPM was towards the cathode ('reverse bias'). The cell was tightened to 3 Nm using a torque wrench. The CO_2 inlet stream was passed through a water saturator at room temperature, at a flow rate of 20 sccm unless specified. The anolyte was pure H_2O, typically 100 mL, recirculated at a rate of 15 mL min^{-1}. All measurements were taken at room temperature (20 – 22 °C). After assembly, the cell was preconditioned at open circuit, with CO_2 and H_2O flowing, for 1 h, before starting electrochemical measurements. The CO_2 inlet flow rate was controlled by a mass flow controller (Alicat), and the outlet stream flow rate was measured using a digital flow meter (Agilent).

Measurement of electroactive coverage was conducted in a one-compartment glass cell with 0.1 M $KHCO_3$ electrolyte, Ag/AgCl reference electrode, Pt wire counter electrode, and Ar purging.

The turnover frequency (TOF) was calculated from the maximum CO partial current density, J_{CO}, and the electroactive coverage, Γ, as follows:

$$TOF = \frac{J_{CO}}{nF\Gamma}$$

where n is 2, and F is Faraday's constant. The electroactive coverage was calculated from integrating the peak area during cyclic voltammetry:

$$\int I\, dE = nFAv\Gamma$$

where n is 1, A is the electrode area, and v is the scan rate.

Electrochemical impedance spectroscopy (EIS) was conducted galvanostatically, with a 20 mA amplitude, with frequencies from 100 kHz to 1 Hz. The cell was held at the operating current for 3 min for equilibration prior to starting the measurement. The equivalent circuit fitting was conducted using the IviumSoft potentiostat control program.

The equilibrium (thermodynamic) voltage was calculated from

cathode: $CO_2 + 2\,e^- + 2H^+ \rightarrow CO + H_2O$ -0.11 V vs RHE

anode: $2H_2O \rightarrow O_2 + 4e^- + 4\,H^+$ 1.23 V vs RHE

yielding $E_{cell,eq}$ = 1.34 V, assuming the same pH at both electrodes.

The voltage requirements for cell resistance and water dissociation resistance were calculated by summing the partial voltages:

$$E = \int_0^{j_{final}} R(j)\, dj \approx \sum_0^{j_{final}} R(j)\, \Delta j$$

Product detection

The outlet stream of the electrolyzer was connected to a gas chromatograph (Varian CP-4900 MicroGC) with a Molsieve 5Å column with Ar carrier gas for H_2 and CO detection by a thermal conductivity detector. The initial injection was taken 2 min after the start of the chronopotentiometry.

Faradaic efficiency calculation:

$$CO\ FE\ (\%) = \frac{Current\ towards\ CO\ production}{Total\ current} = \frac{x v_{out} P/RT}{JA/2F} \times 100$$

where F is Faraday's constant, *J* is current density, *A* is electrode area, v_{out} is the total volumetric outlet flow rate, *x* is the outlet molar fraction of CO, *P* is the pressure, R is the gas constant, and *T* is the temperature.

CO yield calculation:

$$CO\ yield\ (\%) = \frac{CO\ molar\ flow\ out}{CO2\ molar\ flow\ in} = \frac{x v_{out}}{v_{in}} \times 100$$

where *x* is the outlet molar fraction of CO, v_{out} is the total volumetric outlet flow rate, and v_{in} is the inlet volumetric CO_2 flow rate.

Characterization

Scanning electron microscopy (SEM) and energy dispersive X-ray (EDX) measurements were carried out with a Hitachi SEM S4800 at 20 kV. X-ray Photoelectron Spectroscopy (XPS) examinations were carried out using Thermo Scientific K-Alpha X-ray photoelectron spectrometer fitted with Al Kα X-ray source (1486.7 eV). The samples were analysed without further surface cleaning on a spot of 400 x 400 μm^2 area. The survey measurements were recorded in 0-1350 eV range at 200 eV pass energy and the high-resolution scans for elements of interest were obtained in the appropriate range at 50 eV pass energy. The spectra were calibrated by using C 1s peak at 285.0 eV as reference.

Acknowledgements

This work was supported by UKRI-EPSRC (UKRI Interdisciplinary Centre for Circular Chemical Economy**,** EP/V011863/1). The authors acknowledge the Loughborough Materials Characterisation Centre for Pump-Prime Grant 2022 enabling XPS measurements.

Keywords: CO_2 reduction • bipolar membrane • zero-gap electrolyzer • molecular catalyst • water dissociation

References

[1] a)M. G. Kibria, J. P. Edwards, C. M. Gabardo, C.-T. Dinh, A. Seifitokaldani, D. Sinton, E. H. Sargent, *Adv. Mater.* **2019**, *31*, 1807166; b)I. E. L. Stephens, K. Chan, A. Bagger, S. W. Boettcher, J. Bonin, E. Boutin, A. Buckley, R. Buonsanti, E. Cave, X. Chang, S. W. Chee, A. H. M. da Silva, P. De Luna, O. Einsle, B. Endrődi, M. E. Escribano, J. V. Ferreira de Araujo, M. C. Figueiredo, C. Hahn, K. U. Hansen, S. Haussener, S. Hunegnaw, Z. Huo, Y. J. Hwang, C. Janáky, B. S. Jayathilake, F. Jiao, Z. P. Jovanov, P. Karimi, M. T. M. Koper, K. Kuhl, W. H. Lee, Z. Liang, X. Liu, S. Ma, M. Ma, H.-S. Oh, M. Robert, B. R. Cuenya, J. Rossmeisl, C. Roy, M. P. Ryan, E. H. Sargent, P. Sebastián-Pascual, B. Seger, L. Steier, P. Strasser, A. S. Varela, R. E. Vos, X. Wang, B. Xu, H. Yadegari, Y. Zhou, *Journal of Physics: Energy* **2022**; c)A. Somoza-Tornos, O. J. Guerra, A. M. Crow, W. A. Smith, B.-M. Hodge, *iScience* **2021**, *24*, 102813; d)J. Zhang, C. D. Sewell, H. Huang, Z. Lin, *Advanced Energy Materials* **2021**, *11*, 2102767.

[2] a)F. P. García de Arquer, C.-T. Dinh, A. Ozden, J. Wicks, C. McCallum, R. Kirmani Ahmad, D.-H. Nam, C. Gabardo, A. Seifitokaldani, X. Wang, C. Li Yuguang, F. Li, J. Edwards, J. Richter Lee, J. Thorpe Steven, D. Sinton, H. Sargent Edward, *Science* **2020**, *367*, 661-666; b)S. S. Bhargava, F. Proietto, D. Azmoodeh, E. R. Cofell, D. A. Henckel, S. Verma, C. J. Brooks, A. A. Gewirth, P. J. A. Kenis, *ChemElectroChem* **2020**, *7*, 2001-2011.

[3] J. A. Rabinowitz, M. W. Kanan, *Nature Communications* **2020**, *11*, 5231.

[4] a)J. Disch, L. Bohn, S. Koch, M. Schulz, Y. Han, A. Tengattini, L. Helfen, M. Breitwieser, S. Vierrath, *Nature Communications* **2022**, *13*, 6099; b)P. Mardle, S. Cassegrain, F. Habibzadeh, Z. Shi, S. Holdcroft, *J. Phys. Chem. C* **2021**, *125*, 25446-25454; c)M. Sassenburg, M. Kelly, S. Subramanian, W. A. Smith, T. Burdyny, *ACS Energy Letters* **2023**, *8*, 321-331.

[5] A. Ozden, F. P. García de Arquer, J. E. Huang, J. Wicks, J. Sisler, R. K. Miao, C. P. O'Brien, G. Lee, X. Wang, A. H. Ip, E. H. Sargent, D. Sinton, *Nature Sustainability* **2022**, *5*, 563-573.

[6] Y. C. Li, Z. Yan, J. Hitt, R. Wycisk, P. N. Pintauro, T. E. Mallouk, *Advanced Sustainable Systems* **2018**, *2*, 1700187.

[7] a)M. B. McDonald, S. Ardo, N. S. Lewis, M. S. Freund, *ChemSusChem* **2014**, *7*, 3021-3027; b)B. Mayerhöfer, D. McLaughlin, T. Böhm, M. Hegelheimer, D. Seeberger, S. Thiele, *ACS Applied Energy Materials* **2020**, *3*, 9635-9644; c)Z. Yan, T. E. Mallouk, *Accounts of Materials Research* **2021**, *2*, 1156-1166.

[8] B. Pribyl-Kranewitter, A. Beard, T. Schuler, N. Diklić, T. J. Schmidt, *J. Electrochem. Soc.* **2021**, *168*, 043506.

[9] C. P. O'Brien, R. K. Miao, S. Liu, Y. Xu, G. Lee, A. Robb, J. E. Huang, K. Xie, K. Bertens, C. M. Gabardo, J. P. Edwards, C.-T. Dinh, E. H. Sargent, D. Sinton, *ACS Energy Letters* **2021**, *6*, 2952-2959.

[10] J.-B. Vennekoetter, R. Sengpiel, M. Wessling, *Chem. Eng. J.* **2019**, *364*, 89-101.

[11] Z. Yan, J. L. Hitt, Z. Zeng, M. A. Hickner, T. E. Mallouk, *Nature Chemistry* **2021**, *13*, 33-40.

[12] D. A. Salvatore, D. M. Weekes, J. He, K. E. Dettelbach, Y. C. Li, T. E. Mallouk, C. P. Berlinguette, *ACS Energy Letters* **2018**, *3*, 149-154.

[13] K. Xie, R. K. Miao, A. Ozden, S. Liu, Z. Chen, C.-T. Dinh, J. E. Huang, Q. Xu, C. M. Gabardo, G. Lee, J. P. Edwards, C. P. O'Brien, S. W. Boettcher, D. Sinton, E. H. Sargent, *Nature Communications* **2022**, *13*, 3609.

[14] B. Siritanaratkul, M. Forster, F. Greenwell, P. K. Sharma, E. H. Yu, A. J. Cowan, *Journal of the American Chemical Society* **2022**, *144*, 7551-7556.

[15] a)N. Corbin, J. Zeng, K. Williams, K. Manthiram, *Nano Research* **2019**, *12*, 2093-2125; b)Q. Feng, Y. Sun, X. Gu, Z. Dong, *Electrocatalysis* **2022**, *13*, 675-690; c)Z. Chen, G. Zhang, L. Du, Y. Zheng, L. Sun, S. Sun, *Small* **2020**, *16*, 2004158; d)Z. Yue, C. Ou, N. Ding, L. Tao, J. Zhao, J. Chen, *ChemCatChem* **2020**, *12*, 6103-6130; e)F. Lv, N. Han, Y. Qiu, X. Liu, J. Luo, Y. Li, *Coord. Chem. Rev.* **2020**, *422*, 213435.

[16] a)M. N. Mahmood, D. Masheder, C. J. Harty, *J. Appl. Electrochem.* **1987**, *17*, 1223-1227; b)M. Wang, K. Torbensen, D. Salvatore, S. Ren, D. Joulié, F. Dumoulin, D. Mendoza, B. Lassalle-Kaiser, U. Işci, C. P. Berlinguette, M. Robert, *Nature Communications* **2019**, *10*, 3602.

[17] K. Yang, M. Li, S. Subramanian, M. A. Blommaert, W. A. Smith, T. Burdyny, *ACS Energy Letters* **2021**, *6*, 4291-4298.

[18] K. Yang, R. Kas, W. A. Smith, T. Burdyny, *ACS Energy Letters* **2021**, *6*, 33-40.

[19] X. Zhang, Z. Wu, X. Zhang, L. Li, Y. Li, H. Xu, X. Li, X. Yu, Z. Zhang, Y. Liang, H. Wang, *Nature Communications* **2017**, *8*, 14675.

[20] J. Shen, R. Kortlever, R. Kas, Y. Y. Birdja, O. Diaz-Morales, Y. Kwon, I. Ledezma-Yanez, K. J. P. Schouten, G. Mul, M. T. M. Koper, *Nature Communications* **2015**, *6*, 8177.

[21] X. Lu, B. Dereli, T. Shinagawa, M. Eddaoudi, L. Cavallo, K. Takanabe, *Chem Catalysis* **2022**, *2*, 1143-1162.

[22] M. E. Leonard, L. E. Clarke, A. Forner-Cuenca, S. M. Brown, F. R. Brushett, *ChemSusChem* **2020**, *13*, 400-411.

[23] a)Q. Wan, Y. Liu, C. Ke, Y. Zhang, W. Jiang, Y. Qu, L. Zhang, J. Li, J. Gui, J. Hou, G. Xia, J. Yin, J. Zhang, *ACS Sustainable Chemistry & Engineering* **2021**, *9*, 17214-17220; b)C. Sun, Y. Hou, N. Lüdi, H. Hu, M. de Jesús Gálvez-Vázquez, M. Liechti, Y. Kong, M. Liu, R. Erni, A. V. Rudnev, P. Broekmann, *J. Catal.* **2022**, *407*, 198-205.
[24] M. Schmid, A. Kaftan, H.-P. Steinrück, J. M. Gottfried, *Surf. Sci.* **2012**, *606*, 945-949.
[25] M. C. Biesinger, B. P. Payne, A. P. Grosvenor, L. W. M. Lau, A. R. Gerson, R. S. C. Smart, *Appl. Surf. Sci.* **2011**, *257*, 2717-2730.
[26] A. Reyes, R. P. Jansonius, B. A. W. Mowbray, Y. Cao, D. G. Wheeler, J. Chau, D. J. Dvorak, C. P. Berlinguette, *ACS Energy Letters* **2020**, *5*, 1612-1618.
[27] S. A. Hawks, V. M. Ehlinger, T. Moore, E. B. Duoss, V. A. Beck, A. Z. Weber, S. E. Baker, *ACS Energy Letters* **2022**, *7*, 2685-2693.
[28] a)L. Chen, Q. Xu, S. Z. Oener, K. Fabrizio, S. W. Boettcher, *Nature Communications* **2022**, *13*, 3846; b)S. Z. Oener, M. J. Foster, S. W. Boettcher, *Science* **2020**, *369*, 1099-1103; c)S. S. Mel'nikov, O. V. Shapovalova, N. V. Shel'deshov, V. I. Zabolotskii, *Petroleum Chemistry* **2011**, *51*, 577-584; d)M. B. McDonald, M. S. Freund, *ACS Applied Materials & Interfaces* **2014**, *6*, 13790-13797; e)Z. Yan, L. Zhu, Y. C. Li, R. J. Wycisk, P. N. Pintauro, M. A. Hickner, T. E. Mallouk, *Energy & Environmental Science* **2018**, *11*, 2235-2245.
[29] M. C. O. Monteiro, F. Dattila, B. Hagedoorn, R. García-Muelas, N. López, M. T. M. Koper, *Nature Catalysis* **2021**, *4*, 654-662.
[30] Y.-Q. Wang, X.-H. Dan, X. Wang, Z.-Y. Yi, J. Fu, Y.-C. Feng, J.-S. Hu, D. Wang, L.-J. Wan, *Journal of the American Chemical Society* **2022**, *144*, 20126-20133.
[31] I. Bhugun, D. Lexa, J.-M. Savéant, *J. Phys. Chem.* **1996**, *100*, 19981-19985.
[32] S. Sato, K. Sekizawa, S. Shirai, N. Sakamoto, T. Morikawa, *ChemRxiv* **2023**.
[33] M. A. Blommaert, S. Subramanian, K. Yang, W. A. Smith, D. A. Vermaas, *ACS Applied Materials & Interfaces* **2022**, *14*, 557-563.
[34] a)H. Shin, K. U. Hansen, F. Jiao, *Nature Sustainability* **2021**, *4*, 911-919; b)M. J. Orella, S. M. Brown, M. E. Leonard, Y. Román-Leshkov, F. R. Brushett, *Energy Technology* **2020**, *8*, 1900994.

Entry for the Table of Contents

Insert graphic for Table of Contents here. ((Please ensure your graphic is in **one** of following formats))

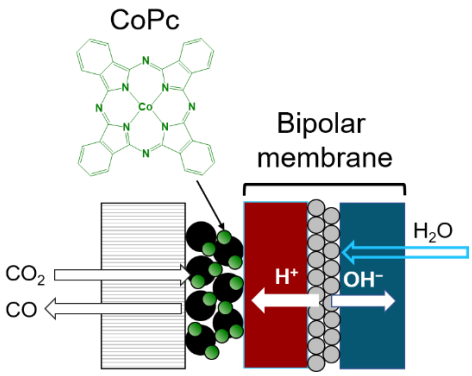

CO_2 electrolyzers are usually operated with a high local pH at the cathode but this can cause issues with bicarbonate salt formation. Operating with a low local pH is desirable but challenging as H_2 evolution can occur. Here we show that a Co molecular catalyst performs with high selectivity and CO_2 utilization in a zero-gap bipolar membrane electrolyzer cell.

Institute and/or researcher Twitter usernames: @AJCowanGroup